Shape-Selective Synthesis and Oxygen Storage Behavior of Ceria Nanopolyhedra, Nanorods, and Nanocubes

Hao-Xin Mai,[†] Ling-Dong Sun,[†] Ya-Wen Zhang,*,[†] Rui Si,[†] Wei Feng,[†] Hong-Peng Zhang,[‡] Hai-Chao Liu,[‡] and Chun-Hua Yan*,[†,§]

State Key Lab of Rare Earth Materials Chemistry and Applications & PKU−HKU Joint Lab on Rare Earth Materials and Bioinorganic Chemistry, Peking University, Beijing 100871, China, and College of Chemistry & Molecular Engineering, Peking University, Beijing 100871, China

Received: September 30, 2005

Single-crystalline and uniform nanopolyhedra, nanorods, and nanocubes of cubic CeO_2 were selectively prepared by a hydrothermal method at temperatures in the range of 100−180 °C under different NaOH concentrations, using $Ce(NO_3)_3$ as the cerium source. According to high-resolution transmission electron microscopy, they have different exposed crystal planes: {111} and {100} for polyhedra, {110} and {100} for rods, and {100} for cubes. During the synthesis, the formation of hexagonal $Ce(OH)_3$ intermediate species and their transformation into CeO_2 at elevated temperature, together with the base concentration, have been demonstrated as the key factors responsible for the shape evolution. Oxygen storage capacity (OSC) measurements at 400 °C revealed that the oxygen storage takes place both at the surface and in the bulk for the as-obtained CeO_2 nanorods and nanocubes, but is restricted at the surface for the nanopolyhedra just like the bulk one, because the {100}/{110}-dominated surface structures are more reactive for CO oxidation than the {111}-dominated one. This result suggests that high OSC materials might be designed and obtained by shape-selective synthetic strategy.

Introduction

Shape-selective synthesis of inorganic nanomaterials is of scientific and technological importance due to their unique shape-dependent material properties and their promising application in catalysis, optoelectronics, microelectronics, magnetics, and biology.[1–10] So far, a number of synthetic approaches including catalytic growth by vapor transport, templating direction, electrochemical deposition, thermolysis of complex precursors in solution phase, and solvothermal/hydrothermal treatments have been developed toward such shape−controlled nanomaterials.[2–9,11–18] Of these methods, hydrothermal treatment has been regarded as one of the most effective and economical routes, as it has the merits of a single step low−temperature synthesis, superior composition and morphological control, and powder reactivity.

As a well-known functional rare earth material, ceria has wide applications in fields such as catalysis, electrochemistry, and optics due to its unique properties.[19–26] For instance, CeO_2 is adopted into three-way catalysts (TWCs) for reducing the emission of the toxic pollutants (CO, NO_x, and hydrocarbons, etc.) from automobile exhaust, because of its high oxygen storage capacity (OSC), associated with its rich oxygen vacancies and low redox potential between Ce^{3+} and Ce^{4+}.[19–22] CeO_2 doped with other rare earth ions has high oxide ion conductivity at a comparable low temperature (about 600 °C) and thus has been applied in solid oxide fuel cells.[23,24] CeO_2 also has strong absorption in the ultraviolet (UV) range and is hence used as

UV blocking and shielding materials.[25–27] In those applications, CeO_2 nanoparticles have significant impact not only due to their considerably small sizes and high surface areas but also due to the general improvements in their material properties with respect to their microsized or bulklike materials.

Recent studies in CeO_2 system have focused on the development of robust synthetic approaches toward size/shape-controlled nanostructures (dots,[25–33] rods,[12,34,35] wires,[36–41] and tubes[42,43]), and the investigation of their size/shape-dependent properties.[25–33,35,41] For example, some groups prepared size−tunable CeO_2 nanocrystals via various wet chemical approaches (including modified precipitation, alcohothermal treatment, microemulsion, and sonochemical method) and investigated their size-dependent UV absorption behavior in order to clarify the confinement effects in CeO_2.[25–33] Li et al. synthesized single-crystalline CeO_2 nanorods by a hydrothermal method, which showed an enhanced CO conversion activity.[35] Chen et al. fabricated polycrystalline CeO_2 nanowires via a solution-phase route using sodium bis(2-ethylhexyl) sulfosuccinate as a structure-directing agent, and observed size-dependent effect on Raman spectra.[41] However, the reports on CeO_2 nanoparticles of different shapes selectively synthesized by the same method are scarce; in particular, the investigation of the shape effects on their material properties (e.g., oxygen storage) has remained a challenge.

Previously, it was well-known that both surface and bulk oxygen atoms could be utilized in the redox process for nanostructured CeO_2 materials, whereas for bulk powders, only surface ones could be used.[21] As we know, the relationship between the OSC and the surface structure associated with a specific crystalline shape for nanometric CeO_2 continues to be a subject of vivid investigation and debate.[19,21,35,44,45] To address this relationship, we think that CeO_2 nanoparticles of different shapes, which have different crystallographic facets and different

---

* Corresponding authors. Telephone and Fax: +86-10-62754179.
† State Key Lab of Rare Earth Materials Chemistry and Applications & PKU−HKU Joint Lab on Rare Earth Materials and Bioinorganic Chemistry, Peking University.
‡ College of Chemistry & Molecular Engineering, Peking University.
§ E-mail: yan@pku.edu.cn.

Ceria Nanopolyhedra, Nanorods, and Nanocubes

J. Phys. Chem. B, Vol. 109, No. 51, 2005 **24381**

TABLE 1: Crystal Structures, Shapes, and Sizes of Several CeO$_2$ Samples^a

no.	C_{NaOH} (mol L^{-1})	T (°C)	t (h)	structure	shape	size (nm)
1	0.01	100	24	cubic	polyhedra	11.5 ± 1.8
2	0.01	180	24	cubic	polyhedra	9−25
3	1	100	24	cubic	polyhedra; rods	
4	3	100	24	cubic	polyhedra; rods	
5	6	100	24	cubic	rods	$(9.6 \pm 1.2) \times (50-200)$
6	6	140	24	cubic	rods; cubes	
7	6	180	24	cubic	cubes	36.1 ± 7.1
8	9	100	24	cubic	rods	$(13.3 \pm 2.8) \times (100-400)$

^{a} Synthesized under [Ce^{3+}] = 0.05 mol L^{-1}.

fraction of surface atoms on their corners and edges, are strongly required. Furthermore, a better understanding in this regard could not only test previous theoretical predications, but also assist in designing CeO$_2$ based OSC materials with high-performance.

In this article, single-crystalline and uniform CeO$_2$ nanopolyhedra, nanorods, and nanocubes of different exposed crystallographic facets have been selectively prepared by a facile hydrothermal method under altered NaOH concentrations, using Ce(NO$_3$)$_3$ as the cerium source. Furthermore, the shape-selective synthetic mechanism, and the shape-dependent OSC behavior are investigated.

Experimental Section

1. Synthesis. All the materials used were of analytical purity. To obtain CeO$_2$ of different shapes, Ce(NO$_3$)$_3$·6H$_2$O (AR grade, Beijing Chem. Corp., China) was used as the cerium source. Then 0.868 g of Ce(NO$_3$)$_3$·6H$_2$O and an appropriate amount of NaOH (0.016−15 g) were dissolved in 5 and 35 mL of deionized water, respectively. Then, these two solutions were mixed in a Teflon bottle, and this mixture was kept stirring for 30 min with the formation of a milky slurry. Subsequently, the Teflon bottle with this mixture was held in a stainless steel vessel autoclave, and the autoclave was sealed tightly. Finally, the autoclave was transferred into a temperature-controlled electric oven, and was subjected to hydrothermal treatment at temperatures in the range of 100−180 °C for 24 h (Table 1). After the hydrothermal treatment, fresh white precipitates were separated by centrifugation, washed with deionized water and ethanol several times, followed by drying at 60 °C in air overnight. The products after drying were yellow powders. The bulk CeO$_2$ powder was prepared by the precipitation route at pH 11 at room temperature, using Ce(NO$_3$)$_3$ and NH$_4$OH as the starting materials, followed by separation, washing, drying, and calcining at 1000 °C for 4 h.

2. Instruments and Charaterization. The powder X-ray diffraction (PXRD) patterns were recorded on a Rigaku D/MAX-2000 diffractometer (Japan) with a slit of 1/2° at a scanning rate of 4° min^{-1}, using Cu Kα radiation (λ = 1.5406 Å). The lattice parameters were calculated with the "LAPOD" software of least-squares refinement of cell dimensions from powder data by Cohen's method.[46,47]

X-ray photoelectron spectrometer (XPS) measurements were carried out in an ion-pumped chamber (evacuated to 2×10^{-9} Torr) of an Escalad5 (U.K.) spectrometer, employing Mg−Kα radiation (BE = 1253.6 eV). The binding energy (BE) for the samples was calibrated by setting the measured BE of C 1s to 284.6 eV. Particle sizes and shapes were examined by a transmission electron microscope (TEM, 200CX, JEOL, Japan) operated at 160 kV. High-resolution TEM (HRTEM) characterization was performed with a Philips Tecnai F30 FEG-TEM operated at 300 kV. The BET specific surface area (S_{BET}) was measured by nitrogen adsorption at 78.3 K, using an ASAP 2010 analyzer (Micromeritics Co. Ltd.), which was performed after

degassing the sample at 373 K for 8 h under vacuum, down to a residual pressure better than 10^{-3} Torr. The samples were calcined at 600 °C for 2 h before the BET determination.

The as-prepared CeO$_2$ nanocrystals were calcined in air at 600 °C for 2 h before OSC measurement. The OSC of the samples were measured at 400 °C under atmospheric pressure in a fixed bed flow microreactor. Then 20 mg of the sample powder was diluted with 200 mg of quartz sand (40−60 mesh) and placed in a quartz tube (6 mm i.d., 55 cm long). After the sample was oxidized at 400 °C in O$_2$ (5%)/He flow for 15 min, and flushed with pure He to remove O$_2$ contamination, CO (5.26% in He) was pulsed into the reactor and the sample was fully reduced at 400 °C by 20 pulses at intervals of 10 min. Afterward, O$_2$ (5% in He) pulses were introduced at the same temperature to complete the reduction−oxidation cycle of the samples. The volume of each pulse was 0.9970 mL. The CO−OSC values were determined by the amount of CO consumed during the CO pulses analyzed by on-line gas chromatography (Shimadzu GC-2010) using a thermal conductivity detector. Each measurement was repeated five times and the results were averaged.

Results and Discussion

1. Characteristics of CeO$_2$ Nanopolyhedra, Nanorods, and Nanocubes. The PXRD patterns of the as-dried CeO$_2$ nanopolyhedra (C_{NaOH} = 0.01 mol L^{-1}, 100 °C, 24 h), nanorods (C_{NaOH} = 6 mol L^{-1}, 100 °C, 24 h), and nanocubes (C_{NaOH} = 6 mol L^{-1}, 180 °C, 24 h) are shown in Figure 1a. The CeO$_2$ nanopolyhedra, nanorods, and nanocubes are of pure cubic phase (fluorite structure, JCPDS 34-0394, space group $Fm-3m$), with lattice constants of 5.414(3), 5.436(3), and 5.405(3) Å, respectively. The broadening of the reflections ascribed to the polyhedra and rods distinctly indicated their nanocrystalline nature, and the sharper reflections for cubes implied their larger sizes as compared with the former two samples.

Figure 1b depicts the XPS spectrum of the CeO$_2$ nanorods. Peaks of Ce 3d, O 1s, C 1s and Ce 4d can be identified. No peaks ascribable to Na 2p are observed, indicating that the NaOH impurity was of trace amount. From the inset in Figure 1b, we can find that six Ce 3d binding energy (BE) peaks for the rods were consistent with the previous report on Ce^{4+}, indicating the main valence of cerium in the rods was +4.[48]

Figure 2a shows the TEM image of the as-obtained uniform CeO$_2$ nanopolyhedra in the size of 11.5 ± 1.8 nm. The HRTEM image in Figure 2b shows the clear (111), (200), and (220) lattice fringes with the interplanar spacing of 0.31, 0.26, and 0.19 nm, respectively, revealing that the CeO$_2$ nanopolyhedra are dominated by a truncated octahedral shape enclosed by the {111} and {100} facets.[49] Figure 2c exhibits the TEM image of the CeO$_2$ nanorods, with a uniform diameter in 9.6 ± 1.2 nm and a less-uniform length within 50−200 nm. Figure 2d depicts the HRTEM image of a CeO$_2$ nanorod combined with a fast Fourier transform (FFT) analysis (inset). According to FFT analysis,
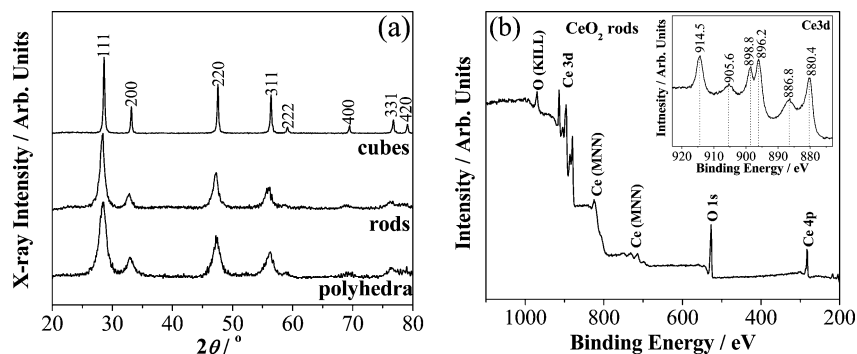
Figure 1. (a) PXRD patterns of CeO$_2$ nanopolyhedra, nanorods and nanocubes. (b) XPS wide spectrum and Ce 3d spectrum (inset) of the CeO$_2$ nanorods.
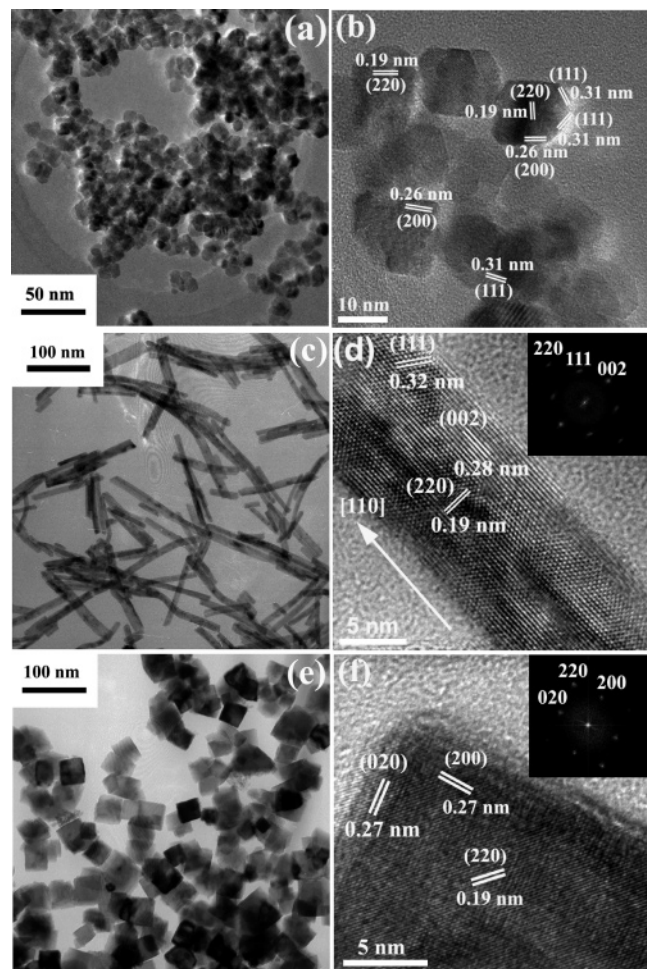

Figure 2. TEM (a) and HRTEM (b) images of CeO$_2$ nanopolyhedra. TEM (c) and HRTEM (d) images of CeO$_2$ nanorods, inset is a fast Fourier transform (FFT) analysis. TEM (e) and HRTEM (f) images of CeO$_2$ nanocubes, inset is a fast Fourier transform (FFT) analysis.

three kinds of lattice fringe directions attributed to (111), (002), and (220) were observed for the nanorods, which have a respective interplanar spacing of 0.32, 0.28, and 0.19 nm on the HRTEM image. The nanorods show a 1D growth structure with a preferred growth direction along [110], and are enclosed by (220) and (200) planes, which are similar to the case of CeO$_2$ nanorods prepared under similar hydrothermal conditions by Li et al.[35] Figure 2e reveals the TEM image of the uniform CeO$_2$ nanocubes with the size of 36.1 ± 7.1 nm. The HRTEM image in Figure 2f combined with FFT analysis (inset) displays the clear (200) and (220) lattice fringes with the interplanar spacing of 0.27 and 0.19 nm, respectively, implying that the
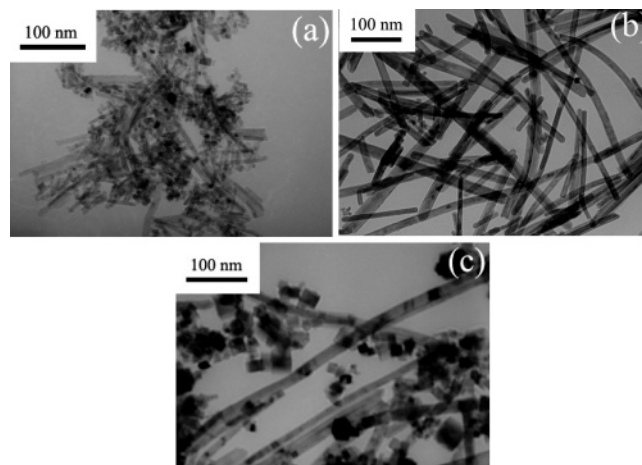

Figure 3. TEM images of CeO$_2$ hydrothermally prepared at 100 °C for 24 h in (a) 3 mol L^{-1} (b) 9 mol L^{-1} NaOH. (c) TEM image of CeO$_2$ hydrothermally prepared at 140 °C for 24 h in 6 mol L^{-1} NaOH.

CeO$_2$ nanocubes are only enclosed by the (200) planes. Such a cube-shape was rarely observed for CeO$_2$ in previous studies.[12,25−43] From the HRTEM images shown in Figure 2, we can also see that the as-obtained CeO$_2$ nanopolyhedra, nanorods, and nanocubes are of single-crystalline nature.

2. Shape-Selective Synthesis and Its Mechanism. Previously, hydrothermal method was employed to prepare CeO$_2$, spherical/angular CeO$_2$ nanoparticles were often obtained in the absence of templating reagents.[49−52] In this work, we found that CeO$_2$ nanopolyhedra, nanorods, and nanocubes could be selectively obtained by changing the base concentration (C_{NaOH}) and hydrothermal temperature (T), using Ce(NO$_3$)$_3$ as the cerium source (Table 1 and Figures 2 and 3). CeO$_2$ nanopolyhedra could be hydrothermally synthesized at a relatively low base concentration (C_{NaOH} = 0.01 mol L^{-1}) at temperatures ranging from 100 to 180 °C. Interestingly, CeO$_2$ nanorods were yielded at a much higher base concentration (C_{NaOH} = 6−9 mol L^{-1}) when hydrothermally treated at 100 °C, whereas, the elevated hydrothermal temperature from 140 to 180 °C led to the formation of CeO$_2$ nanocubes under the same base condition.

According to Table 1, the base concentration and hydrothermal temperature have seemed to be two key factors in the selective formation of CeO$_2$ nanopolyhedra, nanorods, and nanocubes. In the following, series of condition-dependent experiments have been conducted to understand the characteristics of the nucleation and crystal growth processes involved in this synthesis, and further to uncover the underlying shape-selective mechanism.

Generally, the growth habit of crystals always plays an important role in determining their final shape.[8,13,16−18] During
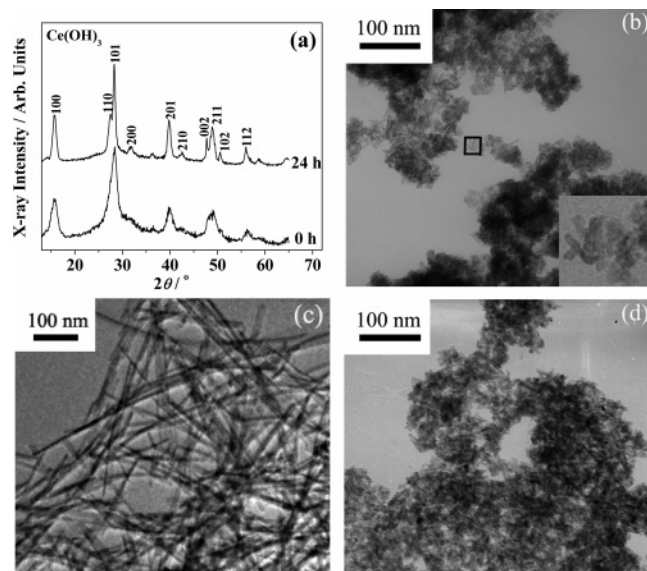
Ceria Nanopolyhedra, Nanorods, and Nanocubes

J. Phys. Chem. B, Vol. 109, No. 51, 2005 **24383**

Figure 4. (a) PXRD patterns of the samples after hydrothermal treatment of as-obtained Ce(OH)$_3$ nuclei at 100 °C for 0 and 24 h in 6 mol L^{-1} NaOH. (b) TEM image of the fresh Ce(OH)$_3$ nuclei (inset was taken from the highlighted section). TEM images of the fresh samples after hydrothermal treatment of the Ce(OH)$_3$ nuclei at 100 °C for 24 h in 6 mol L^{-1} NaOH (c) and in 0.01 mol L^{-1} NaOH (d).

the nontemplate synthesis, the large structural anisotropy of an inorganic compound and its high chemical potential in solution are two main driving forces for the formation of anisotropic nanocrystals.[14,17,18] The materials with anisotropic structures such as CdSe[14] and ZnO[16] easily grow into anisotropic nanocrystals during various solution-phase syntheses without templates, whereas it is difficult for CeO$_2$ to grow anisotropically under the same condition due to its isotropic structure.[25−31,49−52] Nevertheless, the use of capping reagent or template under hydrothermal conditions is more prevalence, as the shape restricted by the nature of crystals is probably broken, especially for the isotropic materials. Thus, various templating methods were developed to prepare CeO$_2$ nanorods and nanowires in solutions.[12,34,36−41]

In the present work, CeO$_2$ nanorods were obtained without addition of any templates. This result strongly suggests that some anisotropic intermediate species must exist during the employed hydrothermal process. Experimentally, we found that the color of the products obtained at 100 °C changed from white to yellow before and after drying, probably indicating that a different structure from cubic one of CeO$_2$ was reserved by the fresh products. Figure 4a depicts the PXRD patterns of the fresh products before and after hydrothermal treatment at 100 °C (C_{NaOH} = 6 mol L^{-1}), showing the (100), (110), (101), (201), and (211) reflections ascribed to hexagonal Ce(OH)$_3$, with the lattice constants of a = 6.50(1) Å and c = 3.814(3) Å (JCPDS 19-0284, space group: $P6_3/m$). Hence, we consider that the intermediate species kept hexagonal structure in the whole hydrothermal process under 100 °C.[12] Figure 4b shows the TEM image of the fresh Ce(OH)$_3$ nuclei. It is noted that they were poorly crystallized, and contained a major portion of rodlike nanoparticles. Because of the large structural anisotropy of Ce(OH)$_3$ nuclei, anisotropic Ce(OH)$_3$ nanocrystals were readily formed during the hydrothermal treatment. After drying, white Ce(OH)$_3$ nanocrystals were converted into yellow CeO$_2$·nH$_2$O ones by air oxidization, without shape changes. Figure 4c revealed the 1D shape of the fresh product (without drying at 60 °C in air overnight), which was similar to that of the as-dried one (see also Figure 2c).

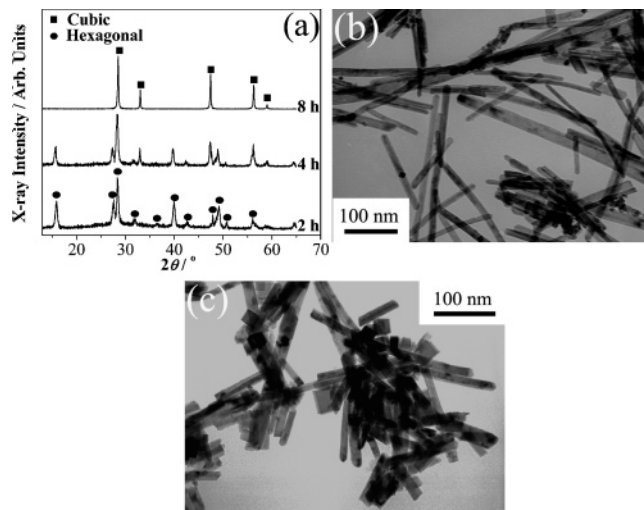**Figure 5.** (a) PXRD patterns of the fresh samples after hydrothermal treatment at 180 °C in 6 mol L^{-1} NaOH for 2−8 h. TEM images of the fresh samples after hydrothermal treatment at 180 °C in 6 mol L^{-1} NaOH for (b) 2 h and (c) 4 h.

Figure 4d shows the TEM image of the sample obtained through hydrothermal treatment of the Ce(OH)$_3$ nuclei in 0.01 mol L^{-1} NaOH at 100 °C for 24 h. We found that the size, shape, and crystallinity of this sample did not show obvious change as compared with those of the nuclei (Figure 4b), implying that the rate of dissolution/recrystallization was quite slow under the low-base concentration. However, when C_{NaOH} was further increased to 6 mol L^{-1}, highly crystallized CeO$_2$ nanorods with a high aspect ratio were obtained, (Figure 4c), due to the greatly accelerated dissolution/recrystallization under the high-base concentration. Moreover, when we changed the cerium source from Ce(NO$_3$)$_3$ to (NH$_4$)$_2$Ce(NO$_3$)$_6$, no nanorods but severely aggregated nanoparticles were obtained (Figure 1S), possibly due to that less-soluble and less-anisotropic CeO$_2$ nuclei, instead of anisotropic Ce(OH)$_3$, were formed directly when Ce^{4+} ions hydrolyzed in the base solution.

At the high base concentrations, as T was raised from 100 to 180 °C, the dissolution/recrystallization associated with the hydrothermal reaction became more vigorous, and resulted in CeO$_2$ nanocubes. On the basis of the PXRD pattern shown in Figure 5a, we can clearly see the occurrence of a phase transition from hexagonal to cubic structure during the hydrothermal treatment at 180 °C in 6 mol L^{-1} NaOH. When hydrothermally treated for 2 h, the nanocrystals were of pure hexagonal structure, suggesting that there were only Ce(OH)$_3$ species in the solution at that time, and the shape of the products were typical nanorods (Figure 5b). However, when the reaction time was extended to 4 h, cubic CeO$_2$ was found (Figure 5a). Considering that some of the Ce(OH)$_3$ species were oxidized into CeO$_2$, both rods and cubes were formed (Figure 5c). When the reaction time was longer than 8 h, Ce(OH)$_3$ was converted into CeO$_2$ totally, and only nanocubes were yielded (Figure 2e). As a result, we suggested that the formation of CeO$_2$ nanocubes under hydrothermal treatment at 180 °C in high C_{NaOH}, was due to not only a greatly accelerated dissolution/recrystallization, but also a transfer step from Ce(OH)$_3$ to CeO$_2$.[51] In this case, the rod shape was metastable, whereas the cube shape was stable. Moreover, when we changed the cerium source from Ce(NO$_3$)$_3$ to (NH$_4$)$_2$Ce(NO$_3$)$_6$, no nanocubes but severely agglomerated nanoparticles were obtained under the same hydrothermal conditions (Figure 1S), proving that the above Ce(OH)$_3$ → CeO$_2$ transition is essential for the formation of CeO$_2$ nanocubes.
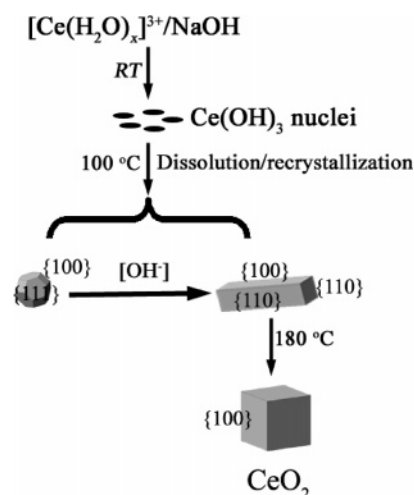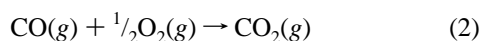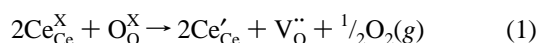
Figure 6. Schematic diagram for the shape-selective synthesis of CeO_2 nanopolyhedra, nanorods and nanocubes. RT stands for room temperature.

According to all the above results, the shape-selective mechanism responsible for the present synthesis of CeO_2 nanopolyhedra, nanorods, and nanocubes (Table 1) can be schematically described in Figure 6. The whole hydrothermal process has been ruled by the well-known dissolution/recrystallization mechanism.[51,52] Anisotropic $Ce(OH)_3$ nuclei formed as soon as the Ce^{3+} ions was mixed with NaOH solution. When hydrothermally treated in low OH^- concentrations ($C_{NaOH} < 1$ mol L^{-1}) at a low temperature of 100 °C, the dissolution/recrystallization rate was slow, and there might exist inadequately high chemical potential for driving the anisotropic growth of the $Ce(OH)_3$ nuclei. Under this condition, CeO_2 nanopolyhedra with enclosing {111} and {100} facets were yielded. When the OH^- concentration was high enough ($C_{NaOH} \geq 1$ mol L^{-1}), the dissolution/ recrystallization rate was considerably promoted so as to drive the $Ce(OH)_3$ nuclei to grow anisotropically; thus, pure CeO_2 nanorods with enclosing {110} and {100} facets were obtained under high base concentrations ($C_{NaOH} \geq 6$ mol L^{-1}). As the hydrothermal temperature rising to 180 °C, $Ce(OH)_3$ became unstable and was readily oxidized into CeO_2. As a result, CeO_2 nanocubes with enclosing {100} facets were produced under such a high base concentration.

3. Oxygen Storage Behavior of CeO_2 Nanopolyhedra, Nanorods, and Nanocubes. The as-obtained CeO_2 nanopolyhedra ($C_{NaOH} = 0.01$ mol L^{-1}, 100 °C, 24 h), nanorods ($C_{NaOH} = 6$ mol L^{-1}, 100 °C, 24 h), and nanocubes ($C_{NaOH} = 6$ mol L^{-1}, 180 °C, 24 h) calcined at 600 °C for 2 h were chosen as the catalysts for CO oxidation reaction, which can be simply written in Kroger and Vink notations as[19]

$$2Ce_{Ce}^X + O_O^X \rightarrow 2Ce'_{Ce} + V_O^{\cdot\cdot} + \tfrac{1}{2}O_2(g) \qquad (1)$$

$$CO(g) + \tfrac{1}{2}O_2(g) \rightarrow CO_2(g) \qquad (2)$$

where Ce_{Ce}^X is the cerium in the lattice of CeO_2, O_O^X is the oxygen in the lattice of CeO_2, Ce'_{Ce} is a Ce^{3+} occupying the site normally occupied by a Ce^{4+} due to the transformation from Ce^{4+} to Ce^{3+}, and $V_O^{\cdot\cdot}$ represents the O^{2-} vacancy produced by the release of O_2.

After the calcination, the shapes of the catalysts nearly kept unchanged (Figure 2S). Table 2 lists the exposed crystal planes (see also Figure 2S), CO−OSC, and the BET specific surface areas of the catalysts. Obviously, all the three CeO_2 nanometric catalysts have much higher OSC than bulk one, due to their

TABLE 2: Exposed Crystal Planes, CO−OSC, and BET Specific Surface Area of the CeO_2 Catalysts

	nanopolyhedron	nanorod	nanocube	bulk
exposed crystals planes	(111) + (100)	(110) + (100)	(100)	
OSC (μmol O g^{-1})	318	554	353	109
S_{BET} (m^2 g^{-1})	62.8	60.8	33.2	0.89
OSC/S_{BET} (μmol O m^{-2})	5.1	9.1	10.6	
calcd OSC (μmol O m^{-2})^a	6.2^b	4.9^b	5.7	

^{a} Calculated according to the theoretical OSC of (100), (110), and (111) surfaces for CeO_2 in the literature, which are 5.7, 4.0, and 6.6 μmol O m^{-2}, respectively.[45] ^{b} Average (equidistribution of the two planes).[45]

significantly increased surface areas.[20,44] CeO_2 nanorods exhibited an OSC of 554 μmol O g^{-1}, which is much higher than that of CeO_2 nanopolyhedra (318 μmol O g^{-1}) despite their comparable surface area close to 62 m^2 g^{-1}. Also, we noticed that the OSC values for CeO_2 nanopolyhedra and nanocubes were comparable, but the surface area of the former was two times higher than the later. As a result, we suggested that the nanocube sample should have much higher CO conversion activity than the nanopolyhedron sample. Among the three catalysts tested, the nanopolyhedron one showed the lowest CO conversion activity.

To estimate the shape effects on the OSC behavior of our samples, the OSC are divided by the surface area, and is also given in Table 2. It is found that the experimental OSC order (in terms of exposed crystal planes) for our CeO_2 samples follows the order of nanocubes > nanorods ≫ nanopolyhedra. In addition, the experimental OSC of CeO_2 nanopolyhedra was 5.1 μmol O m^{-2}, a bit smaller than the calculated value of 6.2 μmol O m^{-2}, indicating that the storage of oxygen on this sample is restricted to the surface, just like the case of bulk CeO_2.[45] However, for our ceria nanorods and nanocubes, their experimental OSC values were nearly two times higher than the calculated ones, indicating that oxygen storage takes place not only at the surface but also in the bulk for these two samples.[45] Further considering that our ceria nanopolyhedra are enclosed by eight (111) and six (100) planes, nanorods enclosed by four (110) and two (100) planes, and nanocubes enclosed by six (100) planes, we can conclude that {100}/{110}-dominated surface structures are much more reactive for CO oxidization and make the associated lattice oxygen migration from bulk to surface much easier than the {111}-dominated one, and the {100}-dominated one is more active than the {110}-dominated one.[45] Similarly, Lundberg et al. found that the more exposure of {100} surfaces in the mesoporous CeO_2 can greatly enhance its CO conversion activity.[53]

As is well-known, CeO_2 holds the fluorite structure (space group: $Fm-3m$), in which, each Ce^{4+} is surrounded by eight equivalent nearest O^{2-} anions forming corners of a cube, and each O^{2-} is surrounded by a tetrahedron of four Ce^{4+} cations. Previous computer modeling shows that the low-index (111) surface has the lowest surface energy and is thus the most stable surface, coming to the (110) surface, and then to high-energy surfaces of (100), (210), and (310).[54,55] Accordingly, the frequently exposed surface in CeO_2 crystals is (111) surface, followed by (110) and (100) surfaces. Sayle et al. predicated that (110) and (310) surfaces are more reactive in the oxidation of CO than (111) due to the ready formation of oxygen vacancies on them.[54] Conesa indicated that less energy is required to form oxygen vacancies on (110) and (100) than on (111).[55] More recently, Sayle et al. found that (100) is more reactive and important catalytically as compared with either (110) or the (111) in the modeling of CeO_2/YSZ(110) system, because of its dipolar nature.[56] Therefore, these theoretical

Ceria Nanopolyhedra, Nanorods, and Nanocubes

J. Phys. Chem. B, Vol. 109, No. 51, 2005 **24385**

results strongly suggest that the exposure of more reactive (100) surfaces, followed by (110) surfaces, should facilitate the formation of oxygen vacancies on them, and enhance the OSC of CeO$_2$ according to the above equations, which are consistent with our experimental results. However, it should be noted that, our OSC results not only confirmed that (100) and (110)-dominated surface structures are more reactive for CO conversion than (111)-dominated one but also revealed that these surface structures facilitate the migration of lattice oxygen from bulk to surface. We think that the later point is worthy of theoretically modeling further.

Conclusion

Using Ce(III) salt as the cerium source, single-crystalline and uniform CeO$_2$ nanopolyhedra, nanorods, and nanocubes were selectively synthesized via a hydrothermal method by changing the NaOH concentration and the reaction temperature. The as-obtained CeO$_2$ nanocrystals showed different exposed crystal planes: {111} and {100} for nanopolyhedra, {110} and {100} for nanorods, and {100} for nanocubes. The whole synthesis was confirmed to take place under the dissolution/recrystallization mechanism, in which hexagonal Ce(OH)$_3$ intermediate species were identified. The formation of Ce(OH)$_3$ and its conversion into CeO$_2$ at elevated hydrothermal temperature, together with the change of NaOH concentration, have been demonstrated to play key roles in the shape evolution. According to the OSC tests at 400 °C, the oxygen storage takes place both at the surface and in the bulk for nanorods and nanocubes, but it is restricted at the surface for nanopolyhedra just like its bulk counterpart, due to the exposure of more reactive (100)/(110) planes for the former two samples. The observation of such a shape-dependent OSC behavior in this work strongly suggest that that high OSC CeO$_2$ materials for TWCs application can be designed by tuning their shapes with specific surface crystallographic facets, i.e., how to enhance the fraction of more reactive {100} and {110} planes, together with decreasing the fraction of less-reactive {111} planes in the nanocrystalline catalysts. In prospect, this work will not only contribute to the development of shape-controlled synthetic methodology for inorganic nanocrystals, but also provides a promise in designing better-performing catalytic materials through shape-selective synthesis strategy.

Supporting Information Available: TEM images of the samples hydrothermally synthesized at 100 and 180 °C in 6 mol L^{-1} NaOH using (NH$_4$)$_2$Ce(NO$_3$)$_6$ as the cerium source (Figure 1S) and TEM and HRTEM images of CeO$_2$ nano-polyhedra, nanorods, and nanocubes after calcining at 600 °C for 2 h (Figure 2S). This material is available free of charge via the Internet at http://pubs.acs.org.

References and Notes

(1) Narayanan, R.; El-Sayed, M. A. *J. Phys. Chem. B* **2005**, *109*, 12663.

(2) Ahmadi, T. S.; Wang, Z. L.; Green, T. C.; Henglein, A.; El-Sayed, M. A. *Science* **1996**, *272*, 1924.

(3) Lisiecki, I. *J. Phys. Chem. B* **2005**, *109*, 12231.

(4) Hu, J. T.; Odom, T. W.; Lieber, C. M. *Acc. Chem. Res.* **1999**, *32*, 435.

(5) Xia, Y. N.; Yang, P. D.; Sun, Y. G.; Wu, Y. Y.; Mayers, B.; Gates, B.; Yin, Y. D.; Kim, F.; Yan, H. Q. *Adv. Mater.* **2003**, *15*, 353.

(6) Wu, Y. Y.; Yan, H. Q.; Huang, M.; Messer, B.; Song, J. H.; Yang, P. D. *Chem.—Eur. J.* **2002**, *8*, 1260.

(7) Alivisatos, A. P. *Science* **1996**, *271*, 933.

(8) Partzke, G. R.; Krumeich, F.; Nesper, R. *Angew. Chem., Int. Ed.* **2002**, *41*, 2446.

(9) Sun, S.; Murray, C. B.; Weller, D.; Folks, L.; Moser, A. *Science* **2000**, *287*, 1989.

(10) Bruchez, M.; Moronne, M.; Gin, P.; Weiss, S.; Alivisatos, A. P. *Science* **1998**, *281*, 2013.

(11) Huang, M. H.; Wu, Y. Y.; Feick, H.; Tran, N.; Weber, E.; Yang, P. D. *Adv. Mater.* **2001**, *13*, 113.

(12) Vantomme, A.; Yuan, Z. Y.; Du, G. H.; Su, B. L. *Langmuir* **2005**, *21*, 1132.

(13) Xu, L. F.; Guo, Y.; Liao, Q.; Zhang, J. P.; Xu, D. S. *J. Phys. Chem. B* **2005**, *109*, 13519.

(14) Peng, Z. A.; Peng, X. G. *J. Am. Chem. Soc.* **2001**, *123*, 1389.

(15) Chen, M.; Xie, Y.; Lu, J.; Xiong, Y. J.; Zhang, S. Y.; Qian, Y. T.; Liu, X. M. *J. Mater Chem.* **2002**, *12*, 748.

(16) Zhang, J.; Sun, L. D.; Yin, J. L.; Su, H. L.; Liao, C. S.; Yan, C. H. *Chem. Mater.* **2002**, *14*, 4172.

(17) Zhang, Y. W.; Yan, Z. G.; You, L. P.; Si, R.; Yan, C. H. *Eur. J. Inorg. Chem.* **2003**, *22*, 4099.

(18) Wang, X.; Li, Y. D. *Angew. Chem., Int. Ed.* **2002**, *41*, 4790.

(19) Trovarelli, A. *Catalysis by Ceria and Related Materials*, 2nd ed.; Dunod: London, 2002.

(20) Powell, B. R.; Bloink, R. L.; Eickel, C. C. *J. Am. Ceram. Soc.* **1988**, *71*, 104.

(21) Kaspar, J.; Fornasiero, P.; Graziani, M. *Catal. Today.* **1999**, *50*, 285.

(22) Si, R.; Zhang, Y. W.; Li, S. J.; Lin, B. X.; Yan, C. H. *J. Phys. Chem. B* **2004**, *108*, 12481.

(23) Steele, B. C. H. *Nature (London)* **1999**, *400*, 619.

(24) Atkinson, A.; Barnett, S.; Gorte, R. J.; Irvine, J. T. S.; Mcevoy, A. J.; Mogensen, M.; Singhal, S. C.; Vohs, J. *Nat. Matter.* **2004**, *3*, 17.

(25) Masui, T.; Fujiwara, K.; Machida, K. I.; Adachi, G. Y. *Chem. Mater.* **1997**, *9*, 2197.

(26) Zhang, Y. W.; Si, R.; Liao, C. S.; Yan, C. H.; Xiao, C. X.; Kou, Y. *J. Phys. Chem. B* **2003**, *107*, 10159.

(27) Si, R.; Zhang, Y. W.; You, L. P.; Yan, C. H. *Angew. Chem., Int. Ed.* **2005**, *44*, 3256.

(28) Inoue, M.; Kimura, M.; Inui, T. *Chem. Commun.* **1999**, 957.

(29) Yin, L. X.; Wang, Y. Q.; Pang, G. S.; Koltypin, Y.; Gedanken, A. *J. Colloid Interface Sci.* **2002**, *246*, 78.

(30) Wang, H.; Zhu, J. J.; Zhu, J. M.; Liao, X. H.; Xu, S.; Ding, T.; Chen, H. Y. *Phys. Chem. Chem. Phys.* **2002**, *4*, 3794.

(31) Zhang, F.; Chan, S.-W.; Spanier, J. E.; Apak, E.; Jin, Q.; Robinson, R. D.; Herman, I. P. *Appl. Phys. Lett.* **2002**, *80*, 127.

(32) Zhang, F.; Jin, Q.; Chan, S.-W. *J. Appl. Phys.* **2004**, *95*, 4319.

(33) Tsunekawa, S.; Fukuda, T. *J. Appl. Phys.* **2000**, *87*, 1318.

(34) Kuiry, S. C.; Patil, S. D.; Deshpande, S.; Seal, S. *J. Phys. Chem. B* **2005**, *109*, 6936.

(35) Zhou, K. B.; Wang, X.; Sun, X. M.; Peng, Q.; Li, Y. D. *J. Catal.* **2005**, *229*, 206.

(36) Tang, B.; Zhuo, L. H.; Ge, J. C.; Wang, G. L.; Shi, Z. Q.; Niu, J. Y. *Chem. Commun.* **2005**, 3565.

(37) Wu, G. S.; Xie, T.; Yuan, X. Y.; Cheng, B. C.; Zhang, L. D. *Mater. Res. Bull.* **2004**, *39*, 1023.

(38) Yada, M.; Sakai, S.; Torikai, T.; Watari, T.; Furuta, S.; Katsuki, H. *Adv. Mater.* **2004**, *16*, 1222.

(39) Yang, R.; Guo, L. *J. Mater. Sci.* **2005**, *40*, 1035.

(40) La, R. J.; Hu, Z. A.; Li, H. L.; Shang, X. L.; Yang, Y. Y. *Mater. Sci. Eng., A* **2004**, *368*, 145.

(41) Sun, C. W.; Li, H.; Wang, Z. X.; Chen, L. Q.; Huang, X. J. *Chem. Lett.* **2004**, *33*, 662.

(42) Yang, R.; Guo, L. *Chin. J. Inorg. Chem.* **2004**, *20*, 152.

(43) Han, W.-Q.; Wu, L.; Zhu, Y. *J. Am. Chem. Soc.* **2005**, *127*, 12814.

(44) Di Monte, R.; Kaspar, J. *Top. Catal.* **2004**, *28*, 47.

(45) Madier, Y.; Descorme, C.; Govic, A. M. L.; Duprez, D. *J. Phys. Chem. B* **1999**, *103*, 10999.

(46) Langford, J. I. *J. Appl. Crystallogr.* **1971**, *4*, 259.

(47) Langford, J. I. *J. Appl. Crystallogr.* **1973**, *6*, 190.

(48) Paparazzo, E.; Ingo, G. M.; Zacchett, N. *J. Vac. Sci. Technol. A* **1991**, *9*, 1416.

(49) Wang, Z. L.; Feng, X. *J. Phys. Chem. B* **2003**, *107*, 13563.

(50) Zhou, Y. C.; Rahaman, M. N. *J. Mater. Res.* **1993**, *8*, 1680.

(51) Hirano, M.; Kato, E. *J. Am. Ceram. Soc.* **1996**, *79*, 777.

(52) Hirano, M.; Kato, E. *J. Am. Ceram. Soc.* **1999**, *82*, 786.

(53) Lundberg, M.; Skårman, B.; Wallenberg, L. R. *Microporous Mesoporous Mater.* **2004**, *69*, 187.

(54) Sayle, T. X. T.; Parker, S. C.; Catlow, C. R. A. *Surf. Sci.* **1994**, *316*, 329.

(55) Conesa, J. C. *Surf. Sci.* **1995**, *339*, 337.

(56) Sayle, D. C.; Maicaneanu, S. A.; Watson, G. W. *J. Am. Chem. Soc.* **2002**, *124*, 11429.